*Materials Research.* 2017; 20(6): 1650-1657
DOI: http://dx.doi.org/10.1590/1980-5373-MR-2017-0568


# Microstructure, Texture and Microhardness Evolution during Annealing Heat Treatment and Mechanical Behavior of the Niobium-Stabilized Ferritic Stainless Steel ASTM 430 and Niobium-Titanium-Stabilized Ferritic Stainless Steel ASTM 439: a Comparative Study

***Leandro Paulo de Almeida Reis Tanure[a]*, Cláudio Moreira de Alcântara[b], Tarcísio Reis de Oliveira[b], Dagoberto Brandão Santos[a], Berenice Mendonça Gonzalez[a]***

*[a]Department of Metallurgical and Materials Engineering, Universidade Federal de Minas Gerais - UFMG, Escola de Engenharia - Bloco 2, Av. Antônio Carlos, 6627, Pampulha, CEP 31270-901, Belo Horizonte, MG, Brazil.*
*[b]Research Department, Aperam South America, Praça 1º de Maio, 09, Centro, CEP 35180-018, Timóteo, MG, Brazil.*

Received: June 08, 2017; Revised: August 08, 2017; Accepted: August 17, 2017

A comparison of the influence of microstructure and texture on mechanical behavior between the niobium-stabilized ferritic stainless steel type ASTM 430, 430Nb, and the niobium-titanium-stabilized ferritic stainless steel type ASTM 439 was performed. The two steels were supplied as cold rolled thin sheets and the annealing was interrupted in different temperatures aiming the characterization of the microstructure and texture in different stages of recrystallization using optical microscopy, Vickers microhardness and Electron Backscatter Diffraction. The annealed samples were tensile tested to determine the mechanical properties and undergone to Swift test to evaluate the drawability. The steel 430Nb showed smaller grain size and greater yield stress. The steel ASTM 439 presented higher normal anisotropy coefficient, $\overline{R}$, and higher Limit Drawing Ratio due to greater proportion of γ fiber. These results are presented and discussed in terms of precipitates and crystallographic texture developed in the recrystallization of both steels.

**Keywords:** *Ferritic stainless steels, mechanical behavior, anisotropy, texture.*

## 1. Introduction

Stainless steels are iron based alloys with, at least, 10.5% of chromium which is responsible for their main property of elevated corrosion resistance due to the formation of a thin, adherent and invisible layer of chromium oxides that regenerates itself in presence of oxygen. The Ferritic Stainless Steels - FSS, because of the lower cost, the lower thermal expansion, the higher thermal conductivity and higher temperature oxidation resistance, compared to the austenitic stainless steels, are used around to world for the most different applications such as home appliances, architecture and automotive industry.[1,2]

In order to minimize the phenomenon of sensitization in FSS is important to keep lower levels of carbon and nitrogen to avoid the formation of chromium carbides and nitrides near the grain boundaries which could leave a chromium depleted zone and promote intergranular corrosion. Besides sensitization, lower plasticity is another factor that limits FSS applications.[3,4]

The control of sensitization can be done adding stabilizing elements such as Titanium, Niobium, Vanadium and Zirconium because they will form precipitates of carbides, nitrides and/or carbonitrides faster and more stable than Chromium. Among these elements, Titanium and Niobium are the best options to reduce sensitization effects. In addition, they improve mechanical resistance without considerable reduction of toughness and ductility due to the reduction of recrystallized grain size.[3,5,6]

Which regards the lower plasticity compared to plain carbon steels and austenitic stainless steels, different metallurgical routes have been created as an attempt to improve the FSS formability. Some studies have shown that elevated values of the average normal anisotropy coefficient, $\overline{R}$, and lower planar anisotropy coefficient, ΔR, promote good deep drawability and are related to a good development of gamma texture.[7,8] Drawability is one of the major requirements for the main applications of FSS[1] and can be achieved increasing the texture levels of gamma fiber and lowering the levels of alpha and theta fibers.[9]

The FSS ASTM 430 stabilized with niobium, 430Nb, present a good combination of mechanical properties and drawability which make them suitable for use that requires good drawability and good superficial finishing.[1] On the other hand, the superficial finishing of FSS ASTM 439, stabilized with titanium and niobium, is not as good as 430Nb, but their drawability is better. Both properties are related to the correct balance between crystallographic texture and grain size.[10,11]

*e-mail: leandrotanure@hotmail.com

In this paper, a comparative study of microstructure, texture and microhardness evolution during recrystallization was performed for the FSS 430Nb and ASTM 439. After recrystallization, mechanical properties and drawability were evaluated. The main objective is to understand and compare how microstructure and texture affect the mechanical behavior. The results could lead and help to develop a new metallurgical route capable of combining the best characteristics of each steel in a single product.

## 2. Experimental Section

*Materials and Methods:* The investigated FSS were ASTM 430 stabilized with niobium, 430Nb, and ASTM 439 (stabilized with titanium and niobium). Their chemical composition (in wt%) are shown in Table 1.

The samples came from hot rolled coils for the steel ASTM 439 while for the steel 430Nb the coil was hot rolled followed by annealing (samples HR). That is the way they are produced in the industry once the hot rolling process for ASTM 439 allows its partial recrystallization and the hot rolling for 430Nb does not. Both samples, with 4.0mm of thickness, were cold rolled until 0.60mm of thickness (samples CR). After that, the annealing treatments were carried out using a heating rate of 24 °C.s$^{-1}$ and soaking time of 24 s. The soaking temperature was 925 °C for the ASTM 439 and 880 °C for 430Nb (samples A). The soaking temperatures were different for each steel due to the industrial process of manufacturing. In addition, samples were taken from five different temperatures during the annealing: 630 °C - samples T1; 700 °C - samples T2; 770 °C - samples T3; 800 °C - samples T4; and 830 °C - samples T5. And then rapidly cooled in cold water to evaluate microstructure, texture and microhardness evolution during different stages of recrystallization. Figure 1 shows a diagram that represents the followed thermo-mechanical process.

*Microstructure Analysis:* The specimens for microstructural analysis followed the standard metallographic procedures (cut, mounting, grinding and polishing) and were taken from the middle of sheets and analyzed through their longitudinal sections. Microstructure evaluation was performed using optical microscopy (LEICA equipment) after etch with the etchant Villela for 50s.

For the annealed specimens (samples A), Scanning Electron Microscopy (SEM - FEI Inspect S50) analysis were made and grain size were measured with Abrams Concentric Circles method according to the standard ASTM E112-13.[12] Some precipitates, for a qualitative evaluation, were measured using the software Image-PRO®.

*Texture Analysis:* Regarding texture analysis preparation, besides the standard metallographic procedure, an additional step of polishing using colloidal silica was required. The samples were analyzed using the method of Electron Backscatter Diffraction (EBSD) in their longitudinal sections with the aid of FEI-Quanta 200 FEG electron microscope and the software OIM®. The hot rolled samples and the annealed samples were analyzed through their whole thickness while the others were analyzed in a field of 50x100 μm located at the middle of the thickness.

*Mechanical Properties:* Tensile tests were carried out, at room temperature, on the annealed samples (samples A) using an INSTRON 5583 equipment. The yield strength (YS) and ultimate tensile strength (UTS) were measured following the standard ASTM A370-10.[13] To evaluate the anisotropy of the sheets, the average normal anisotropy coefficient, $\overline{R}$, was calculated using the Equation 1

$$\frac{R_0 + 2R_{45} + R_{90}}{4} \quad (1)$$

where $R_0$, $R_{45}$ and $R_{90}$ correspond to the R-value in the directions of 0°, 45° and 90° to the rolling direction, respectively. In addition, the planar anisotropy coefficient, ΔR, was evaluated using the Equation 2.

$$\frac{R_0 - 2R_{45} + R_{90}}{2} \quad (2)$$

The samples were strained by 15% and the anisotropy tests were performed according to ASTM E517-10[14] standard. The deep drawability of the annealed specimens was evaluated in a Swift test using an Erichsen 14240 equipment to determine the Limit Drawing Ratio (LDR).

Vickers microhardness tests were performed to evaluate microhardness evolution during all the steps of the proposed study. For each specimen, twenty indentations were randomly made using a Leitz-Wetzlar microhardness tester.

## 3. Results and Discussion

### *3.1 Microstructure Analysis*

Microstructures of cold rolled samples (CR) are shown in Figure 2 and demonstrate highly deformed grains after the 85% reduction in thickness (4.0mm to 0.60mm) in both steels, which is characteristic from the deformed state.

The microstructure of the specimens whose annealing treatment were interrupted at temperatures T1, 630 °C, T2, 700 °C, and T3, 770 °C, remained practically unchanged for both steels. Until the temperature of 770 °C, it was not

**Table 1.** Chemical compositions [wt%] of the investigated steels.

| Steel | C | Mn | Si | Cr | N | Ni | Nb | Ti |
|---|---|---|---|---|---|---|---|---|
| **430Nb** | 0.017 | 0.17 | 0.34 | 16.5 | 0.022 | 0.23 | 0.31 | - |
| **ASTM439** | 0.010 | 0.19 | 0.50 | 17.2 | 0.011 | 0.20 | 0.19 | 0.15 |

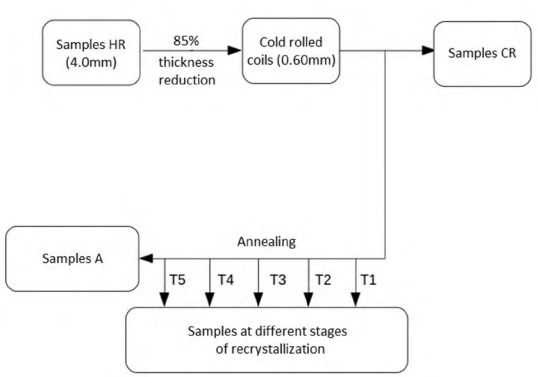


**Figure 1.** Thermo-mechanical processing scheme.

possible to identify any changes in microstructure analyzed by optical microscopy.

Regarding conditions T4, 800°C, and T5, 830°C, microstructures are shown in Figure 3. As can be seen in Figure 3 (a) and (d), the recrystallization phenomena has begun at T4 condition, 800 °C, for steel 430Nb and at T5 condition, 830 °C, for ASTM 439 steel. The black arrows indicate new grains at the beginning of the recrystallization for each steel at different temperatures in a highly deformed ferritic microstructure matrix.

Figure 4 shows the final microstructure for the annealed samples (samples A). Regarding the annealed specimens, steel 430Nb presented a grain size of (15±1) µm while the steel ASTM 439 presented a grain size of (19±1) µm. The prior recrystallization in 430Nb steel and its lower ferritic grain size can be related to three different factors: the lower annealing temperature and the higher content of interstitial elements (both lead to small grains) and the lower level of atoms in solid solution (promotes a faster recrystallization once there is less atoms which could migrate to grain boundaries reducing their mobility).

The lower annealing temperature, 880 °C for 430Nb steel and 925 °C for ASTM 439 was responsible for providing a higher supercooling which increases the driving force for the formation of a fine distribution of precipitates. Besides the temperature effect, the smaller grain size is consequence of the elevated level of carbon and nitrogen on 430Nb steel (C+N~400 ppm) that precipitate and stimulate the nucleation of new grains. The effect of interstitial elements on amount and distribution of precipitates can be seen on SEM images on Figure 5.

There are more precipitates in steel 430Nb and, in both specimens, coarse precipitates are located preferentially in grain boundaries while the fine ones are either in grain boundaries or in the ferritic matrix. The presence of precipitates greater than 1µm increases the nucleation rate of new grains by the mechanism of Particle Stimulated Nucleation while the smaller precipitates decrease the growing rate of the same grains because they difficult the movement of grain boundaries by pinning effect.[16] The combination of these two effects leads to smaller grain size in the 430Nb steel. The bigger precipitates range from 4 µm to 6 µm on steel 430Nb and from 4 µm to 10 µm on ASTM 439.

The amount of niobium and titanium atoms in solid solution also affects the recrystallization and can be calculated according the Equation 3 and 4 for bi-stabilized steels (ASTM 439) [17] and the amount of niobium according Equation 5 for mono-stabilized steels (430Nb)[17]

$$\Delta Nb = \%Nb - 7.74 * 0.7\%C \quad (3)$$

$$\Delta Ti = \%Ti - 4.0 * 0.3\%C - 3.42\%N \quad (4)$$

$$\Delta Nb = \%Nb - 6.6\%N - 7.74\%C \quad (5)$$

The amounts of niobium in solid solution (weight%) were 0.037 and 0.13 for the steels 430Nb and ASTM 439, respectively, while the amount of titanium in solid solution was 0.10 for steel ASTM 439. The lower level of solid solution

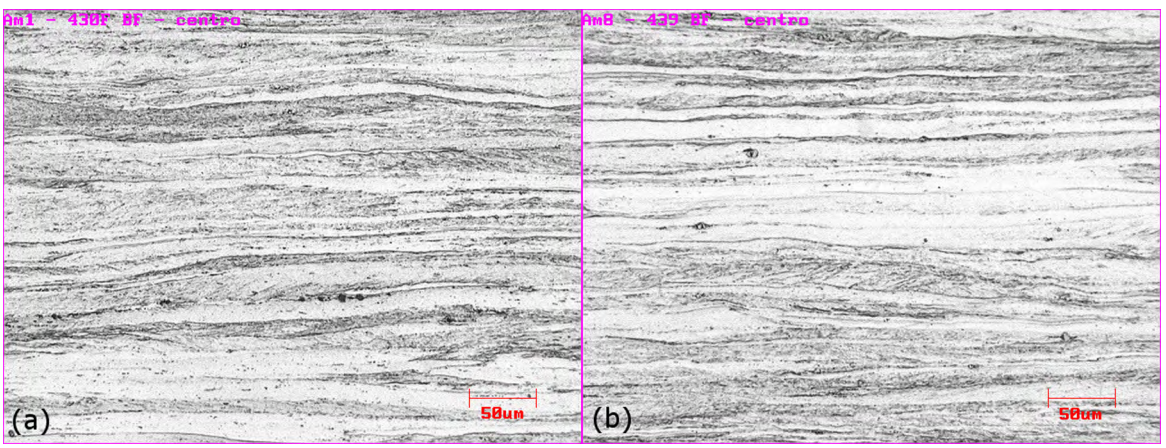


**Figure 2.** Microstructure of the cold rolled samples (CR). (a) 430Nb CR and (b) ASTM 439 CR

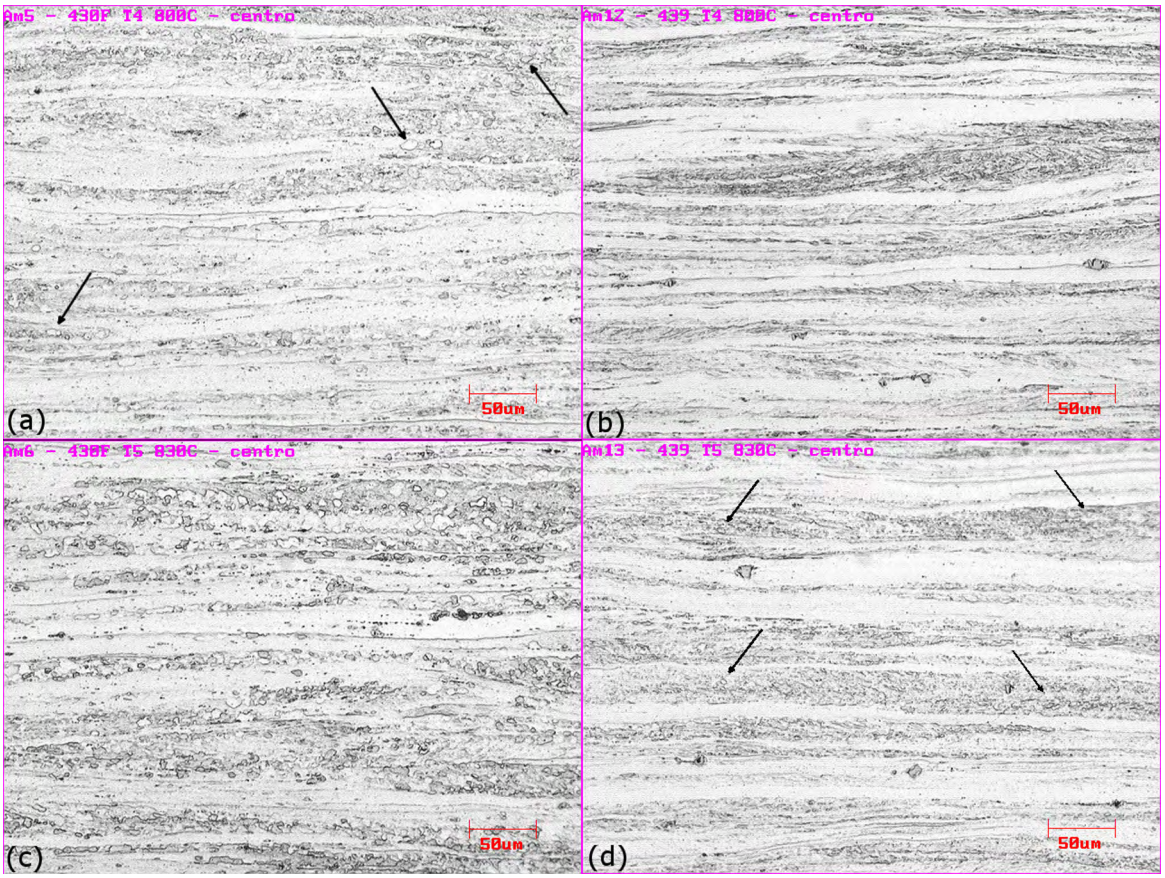


**Figure 3.** Microstructure of the samples with interrupted annealing treatment at temperatures T4, 800 °C, (a) 430Nb T4 (b) ASTM 439 T4 and T5, 830 °C, (c) 430Nb T5 (d) ASTM 439 T5.

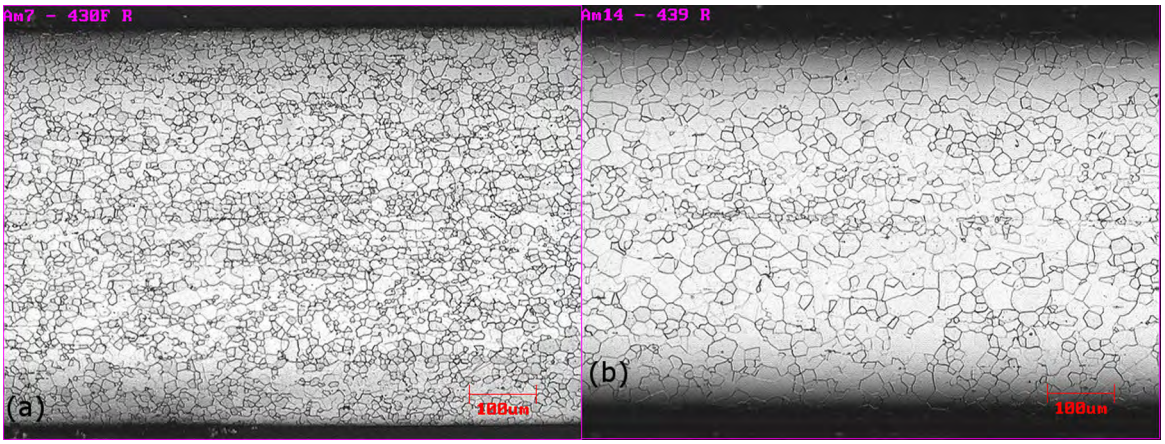


**Figure 4.** Microstructure of the samples after annealing treatment (a) 430Nb A (b) ASTM 439 A.

atoms in 430Nb steel promoted a faster recrystallization under lower temperatures, since solid solution atoms tend to migrate to grain boundaries decreasing either nucleation and growing rates.[18]

### *3.2 Texture Analysis*

The Orientation Distribution Functions (ODFs) of hot rolled samples are shown in Figure 6 and demonstrate that both specimens presented strong texture in Goss component (110)[001]. 430Nb steel showed strong texture components lying on α fiber with major component near (112)[$1\bar{1}0$] direction while ASTM 439 steel showed weak components along γ fiber.

Lee et al.[19] showed that specific texture components present differences regarding the R Lankford coefficient. The component Rotated Cube, {001}<110>, has lower values while the Goss component, {110}<001>, presents a greater variation of R-values as function of rolling direction, which

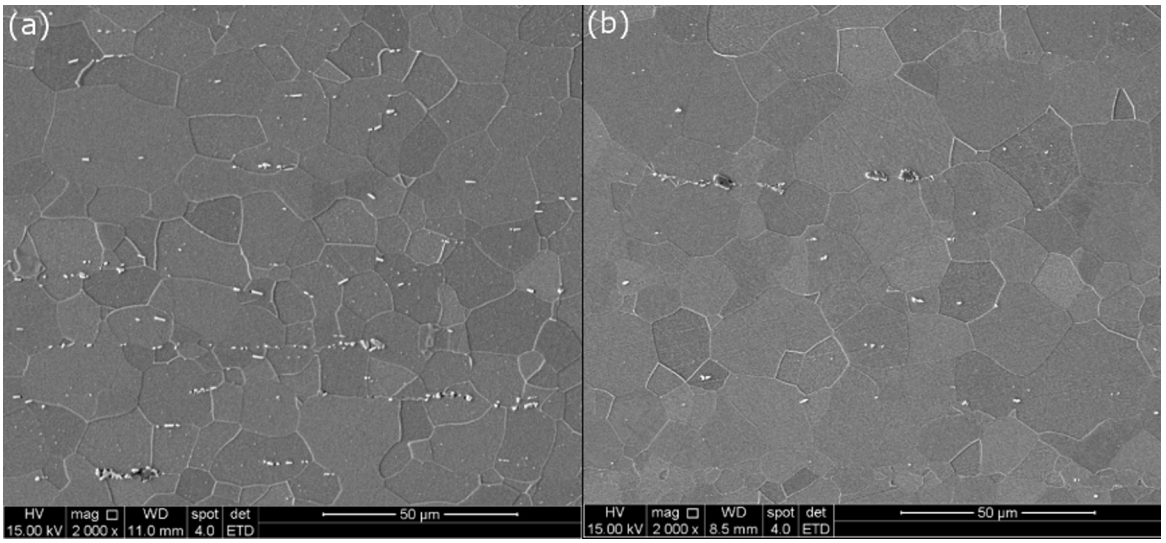


**Figure 5.** Precipitates of the annealed specimens (a) 430Nb A (b) ASTM 439 A. [15]

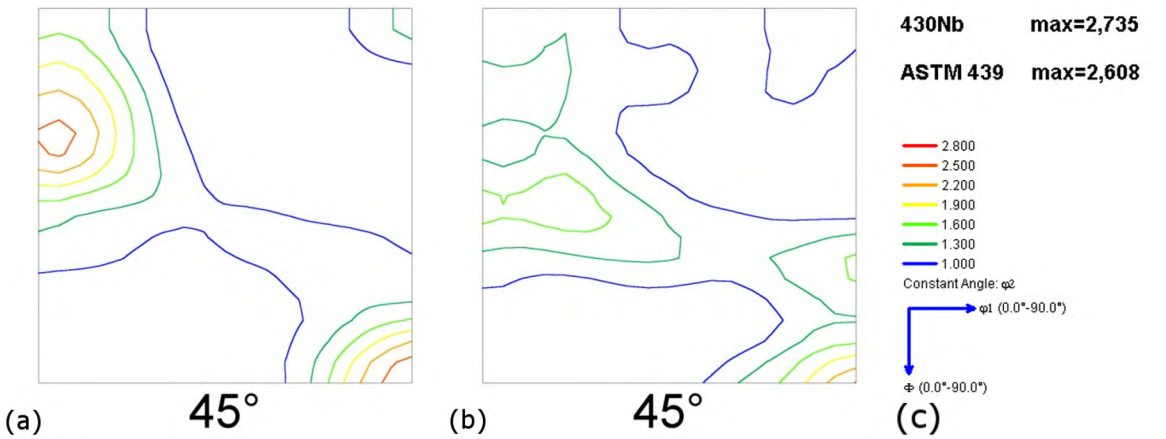


**Figure 6.** ODFs maps of hot rolled samples (HR). (a) 430Nb steel. (b) ASTM 439 steel. (c) levels. Constant sections of φ2=45º.

makes it difficult to control and keep R coefficient under elevated values. A combination of components {111}<112> and {111}<110>, both of them belonging to γ fiber, is the best option which concerns drawability requirements (because it leads to a higher average normal anisotropy coefficient, $\overline{R}$, and lower planar anisotropy coefficient, ΔR).

Starting from cold rolled condition, it is possible to follow the texture evolution (for conditions CR, T1, T2, T4, T5 and A) for both steels during the annealing treatment in Figure 7 and 8.

As can be seen in Figure 7, there were changes in texture components, basically, in fibers α, γ and Rotated Cube component. During recrystallization is expected a reduction of α fiber level and a consequent increase in γ fiber level. In the annealed sample, Figure 7 (f), there is almost none component related to Rotated Cube, which was predicted by Lee et al.[8] due to intermediate annealing treatment, which was applied in this steel after hot rolling, and is able to reduce the development of Rotated Cube component after final annealing. It highlights the importance and the effect of previous texture on the final recrystallized texture.

Figure 8 shows the texture evolution for specimens of ASTM 439 steel during the annealing heat treatment. The behavior of texture evolution was similar in both steels. The variations regarding fibers and texture components were, practically, restricted to α and γ fiber and Rotated Cube component. Among all conditions analyzed, the annealed sample of the ASTM 439 steel, Figure 8 (f), presented the lowest intensities of α fiber and highest levels of γ fiber. Differences of behavior are due to precipitates characteristics. Since titanium precipitates, such as TiN, are more stable and remains practically unchanged during the annealing heat treatment[20] and niobium precipitates are more likely to change in lower temperatures[21], some differences during recrystallization are expected.

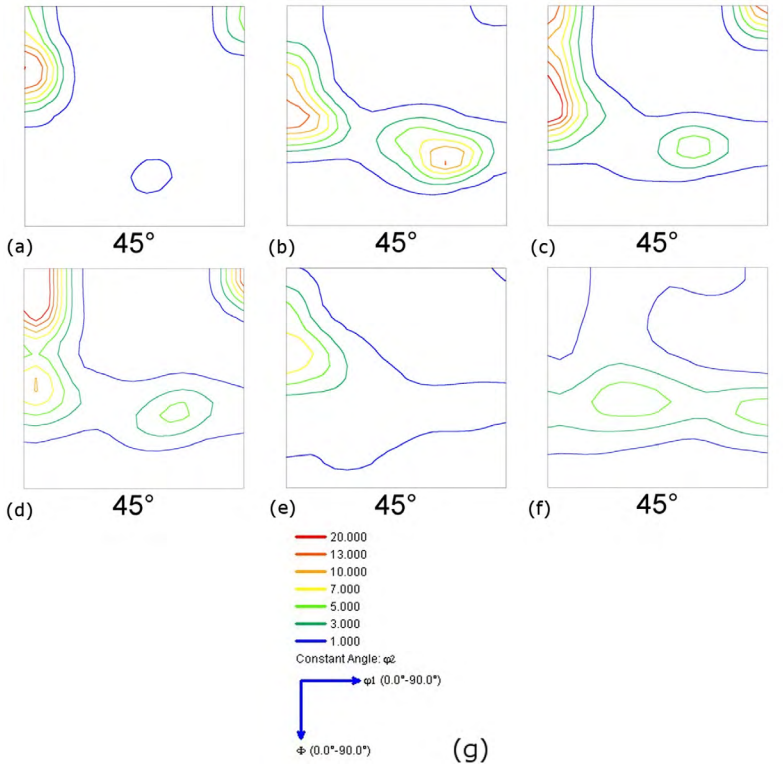


**Figure 7.** ODFs maps for specimens of the 430Nb steel at conditions (a)CR, (b)T1, (c)T2, (d) T4, (e)T5 and (f)A, respectively. (g) levels. Constant sections of φ2=45º

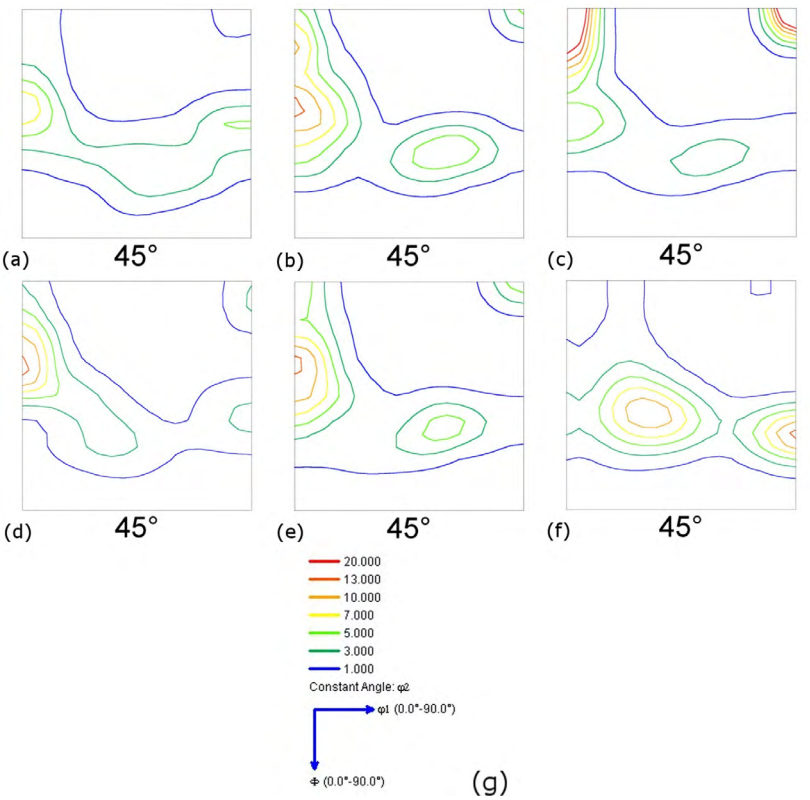


**Figure 8.** ODFs maps for specimens of the ASTM 439 steel at conditions (a)CR, (b)T1, (c)T2, (d)T4, (e)T5 and (f)A, respectively. (g) levels. Constant sections of φ2=45º

**Table 2.** Tensile properties and drawability results for the studied steels.

| Tensile properties | | YS [MPa] | UTS [MPa] | Uniform elongation [%] | | |
|---|---|---|---|---|---|---|
| **430Nb** | | 291 ± 4 | 460 ± 3 | 22 ± 3 | | |
| **ASTM 439** | | 281 ± 3 | 465 ± 2 | 22.8 ± 0.2 | | |
| **Drawability** | $R_0$ | $R_{45}$ | $R_{90}$ | $\overline{R}$ | ΔR | LDR |
| **430Nb** | 1.45±0.01 | 1.09±0.04 | 1.36±0.18 | 1.25±0.03 | 0.31±0.13 | 2.18 |
| **ASTM 439** | 1.86±0.02 | 1.73±0.11 | 2.15±0.05 | 1.87±0.05 | 0.28±0.14 | ≥2.30 |

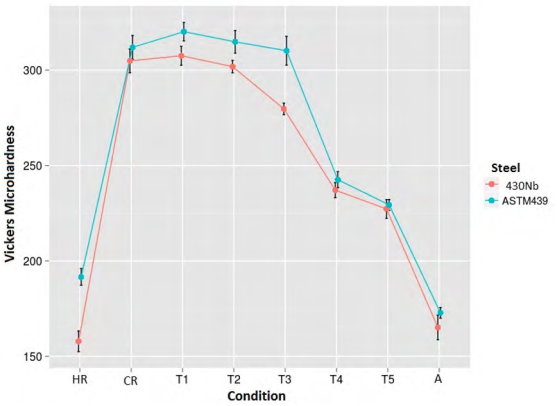


**Figure 9.** Mean values of Vickers microhardness for steels 430Nb and ASTM 439 in different conditions.

Once γ fiber presents a higher Taylor factor compared to fibers α and θ (which are deleterious for drawability requirements), grains with orientations that belongs to γ fiber will be more likely to replace those grains oriented according α and θ fibers during annealing[22]. In both steels this behavior should be expected, such as when cold rolled and annealed conditions are compared (decrease in α fiber and increase in γ fiber). Little deviations are also expected because the analyzed field was very small (50x100 μm) and could not be the best field to represent that specific condition.

The size and distribution of precipitates affects recrystallization texture. Lower annealing temperatures promoted the formation of a higher number and homogeneous dispersed precipitates, which led to nucleation of smaller grains with a random crystallographic orientation weakening the γ fiber, once they suppress the growth of preferentially nucleated grains[23]. On the other hand, coarse and widely distributed precipitates do not tend to dramatically change texture. The greater amount of fine precipitates on 430Nb steel does not let the γ fiber develop as well as on ASTM 439 steel.

### *3.3 Mechanical Properties*

*Vickers Microhardness:* The mean values of Vickers microhardness obtained for all conditions were plotted in Figure 9 with their respective bars that represent the confidence level of 95%.

ASTM 439 steel presented higher Vickers microhardness mean values for all analyzed conditions, but according to Figure 9, only conditions T1, T2 and T3 presented statistical difference between steels 430Nb and ASTM 439. The faster softening of 430Nb steel indicates the occurrence of a faster recrystallization because of the formation of new grains strain free. This observation is in accordance with microstructure analysis and corroborates the thesis of prior recrystallization in 430Nb steel.

*Tensile Properties.* The results provided by tensile test are shown in Table 2. The value for yield stress was slightly higher for the 430Nb steel due to the smaller grain size. The ultimate tensile strength and the uniform elongation remains approximately the same for both steels considering the mean error.

*Drawability:* The drawability was evaluated through the average normal anisotropy coefficient value, $\overline{R}$, the planar anisotropy coefficient, ΔR, and Limit Drawing Ratio, LDR. The results are shown in Table 2. The more elevated average normal anisotropy coefficient, $\overline{R}$, which means a better resistance concerning thickness thinning, leads to choose ASTM 439 when the drawability performance is the major requirement. The LDR result also indicates that it is possible to draw deepest blanks using this steel. This behavior was expected once ASTM 439 presented a more pronounced texture on γ fiber and almost none texture components related to α fiber texture if compared to 430Nb steel. Considering the mean error, there was no difference for the planar anisotropy coefficient, ΔR.

## 4. Conclusion

The 430Nb steel presented a smaller recrystallized grain size due to three factors: the greater volume fraction of precipitates (because of the higher amount of carbon and nitrogen); the lower annealing temperature, which provides higher driving force for precipitates formation, and due to the reduced amount of atoms in solid solution promoting a faster recrystallization.

During the annealing, there were changes in texture according to fibers α, γ and the Rotated Cube component. For both steels, it was observed reduction in fiber α and Rotated Cube component and an increase in γ fiber. The presence of more precipitates in 430Nb steel does not allow the strengthening of γ fiber during recrystallization due to the smaller and randomly oriented grains.

After the annealing heat treatment, the higher intensity of texture components related to γ fiber on ASTM 439 steel led to better results concerning drawability requirements. It showed a more elevated value for average normal anisotropy coefficient, $\overline{R}$, and LDR.

## 5. Acknowledgements

The authors are grateful for financial support by Coordenação de Aperfeiçoamento de Pessoal de Nível Superior (CAPES), Conselho Nacional de Desenvolvimento Científico e Tecnológico (CNPq), Fundação de Amparo à Pesquisa do Estado de Minas Gerais (FAPEMIG), Pró-Reitoria de Extensão da Universidade Federal de Minas Gerais (PROEX/UFMG) and technical support by Aperam South America. The authors would like to acknowledge the Center of Microscopy at the Universidade Federal de Minas Gerais (http://www.microscopia.ufmg.br) for providing the equipment and technical support for experiments involving electron backscatter diffraction.

## 6. References

1. International Stainless Steel Forum (ISSF). *The Ferritic Solution - Properties, Advantages and Applications: The Essential Guide to Ferritic Stainless Steels*. Brussels: ISSF; 2007.

2. Lo KH, Shek CH, Lai JKL. Recent developments in stainless steels. *Materials Science and Engineering: R: Reports*. 2009;65(4-6):39-104.

3. You XM, Jiang ZH, Li HB. Ultra-Pure Ferritic Stainless Steels-Grade, Refining, Operation and Application. *Journal of Iron and Steel Research, International*. 2007;14(4):24-30.

4. Krauss G. *Steels: Processing, Structure and Performance*. 1st ed. Materials Park: ASM International; 2005.

5. Cavazos JL. Characterization of precipitates formed in a ferritic stainless steel stabilized with Zr and Ti additions. *Materials Characterization*. 2006;56(2):96-101.

6. Yan H, Bi H, Li X, Xu Z. Microstructure and texture of Nb + Ti stabilized ferritic stainless steel. *Materials Characterization*. 2008;59(12):1741-1746.

7. Du W, Jiang X, Sun Q, Liu Z, Zhang X. Microstructure, Texture and Formability of Nb+Ti Stabilized High Purity Ferritic Stainless Steel. *Journal of Iron and Steel Research, International*. 2010;17(6):47-52.

8. Lee KM, Huh MY, Park S, Engler O. Effect of Texture Components on the Lankford Parameters In Ferritic Stainless Steel Sheets. *ISIJ International*. 2012;52(3):522-529.

9. Engler O, Randle V. *Introduction to Texture Analysis: Macrotexture, Microtexture and Orientation Mapping*. 2nd ed. Boca Raton: CRC Press; 2009.

10. Wu PD, Jin H, Shi Y, Lloyd DJ. Analysis of ridging in ferritic stainless steel sheet. *Materials Science and Engineering: A*. 2006;423(1-2):300-305.

11. Shu J, Bi H, Li X, Xu Z. Effect of Ti addition on forming limit diagrams of Nb-bearing ferritic stainless steel. *Journal of Materials Processing Technology*. 2012;212(1):59-65.

12. ASTM International. *ASTM E112-13 - Standard Test Methods for Determining Average Grain Size*. West Conshohocken: ASTM International; 2013.

13. ASTM International. *ASTM A370 - Standard Test Methods and Definitions for Mechanical Testing of Steel Products*. West Conshohocken: ASTM International; 2010.

14. ASTM International. *ASTM E517-00 - Standard Test Methods for Plastic Strain Ratio r for Sheet Metal*. West Conshohocken: ASTM International; 2010.

15. Tanure LPAR, Alcântara CM, Oliveira TR, Santos DB, Gonzalez BM. Comparison of Microstructure and Mechanical Behavior of the Ferritic Stainless Steels ASTM 430 Stabilized with Niobium and ASTM 439 Stabilized with Niobium and Titanium. *Materials Science Forum*. 2016;879:1651-1655.

16. Humphreys FJ, Hatherly M. *Recrystallization and Related Annealing Phenomena*. 2nd ed. Oxford: Elsevier; 2004.

17. Oliveira TR. *Effet du niobium et du titane sur la déformation à chaud d'aciers inoxydables ferritiques stabilisés*. [PhD]. Saint-Étienne: l'Ecole Nationale Supérieure des Mines de Saint-Étienne, l'Université Jean Monnet de Saint-Étienne; 2003.

18. Abbaschian R, Abbaschian L, Reed-Hill RE. *Physical Metallurgy Principles*. 4th ed. Stamford: Cengage Learning; 2009.

19. Lee KM, Park J, Kim S, Park S, Huh MY. Quantification od ridging in ferritic stainless steel sheets by electron backscattered diffraction R-value maps. *Microscopy and Microanalysis*. 2013;19 Suppl 5:17-20.

20. Najafi H, Rassizadehghani J, Halvaaee A. Mechanical properties of as cast microalloyed steels containing V, Nb and Ti. *Materials Science and Technology*. 2007;23(6):699-705.

21. Malfliet A, Mompiou F, Chassagne F, Mithieux JD, Blanpain B, Wollants P. Precipitation in Nb-Stabilized Ferritic Stainless Steel Investigated with *in-situ* and *ex-situ* Transmission Electron Microscopy. *Metallurgical and Materials Transactions A*. 2011;42:3333-3343.

22. Han J, Li H, Zhu Z, Jiang L, Xu H, Ma L. Effects of processing optimisation on microstructure, texture, grain boundary and mechanical properties of Fe-17Cr ferritic stainless steel thick plates. *Materials Science & Engineering: A*. 2014;616:20-28.

23. Gao F, Liu ZY, Wang GD. Effect of the size and dispersion of precipitates formed in hot rolling on recrystallization texture in ferritic stainless steels. *Journal of Materials Science*. 2013;48(6):2404-2415.